Intergalactic HI and OVI:
A Survey of 259 low-z COS Absorbers with Reference to Ionization Mechanics

by

Shannon Osborne

A thesis submitted to the faculty of the University of Colorado
in partial fulfillment of the requirements for the award of departmental
honors in the Department of Astrophysical and Planetary Sciences

Committee Members:

Advisor: Dr. Charles Danforth, Dept. of Astrophysical and Planetary Sciences

Dr. Erica Ellingson, Dept. of Astrophysical and Planetary Sciences

Dr. Paul Beale, Dept. of Physics

April 3, 2017

Abstract

Modern astrophysics still lacks a strong understanding of the Intergalactic Medium (IGM), particularly the Warm-Hot Intergalactic Medium (WHIM; T = 10^5 – 10^7 K). To better understand the distribution and temperature of this gas, absorption-line observations along AGN sight lines from the Cosmic Origins Spectrograph onboard the Hubble Space Telescope (COS/HST) were analyzed (see Danforth et al. 2016). Here we present the largest analysis to date of IGM systems detected in both HI and OVI: 259 absorbers along 52 sight lines. We separate these systems into aligned and non-aligned categories based on the velocity separation of the HI and OVI absorption features. For the aligned HI and OVI absorption, we derive a median temperature of $logT$ = 4.65 (with a ±1σ range of 4.22 – 5.03 in Kelvin) and a median value for the non-thermal motions in the clouds of b_{NT} = 22 km/s (with a ±1σ range of 17 – 34 km/s). This temperature is lower than expected for collisional ionization equilibrium and suggests that most aligned IGM OVI absorbers are either photoionized or originally shock-heated but then cooled (non-equilibrium ionization). After finding no difference in the distribution of the other physical parameters (e.g. column density) between the aligned and non-aligned systems, we use the distribution of non-thermal b-values to statistically derive temperature for the HI and OVI absorbers in the non-aligned cases which results in $logT_{HI}$ = 4.80 (with a ±1σ range of 4.44 – 5.11) and $logT_{OVI}$ = 5.99 (with a ±1σ range of 5.50 – 6.31). The higher OVI temperature distribution found here points to these non-aligned clouds being more likely collisionally ionized.

Acknowledgments

I would like to acknowledge the following people:

Dr. Charles Danforth for being an amazing, insightful, and supportive mentor

All my professors over the last four years who have inspired me

Susan Armstrong for being Astro Mom and always having chocolate on hand in case of emergencies (of which there were many)

My family and friends for their constant love and support as I spent all my evenings and weekends in the library

My committee members for taking the time to read my thesis

Table of Contents:

1.0 Introduction

1.1 The Missing Baryon Problem

In the astrophysical community, the Missing Baryon Problem is a well-known disparity between simulations and observations. Using big bang nucleosynthesis and deuterium measurements (e.g. O'Meara et al. 2006) and the Cosmic Microwave Background (CMB; e.g. Spergel et al. 2007), astronomers have been able to predict the baryon density in the early universe. However, in the low-redshift (low-z), more current universe, there appears to be a baryon deficiency (Fukugita, Hogan, & Peebles 1998). This deficit is most likely due to having an incomplete inventory of low-z baryons.

While most would think that galaxies contain the majority of the universe's baryons, in fact ~80% of the baryons in the low-z universe are found outside of galaxies, and thus must be in the Intergalactic Medium (IGM; Danforth & Shull 2005, 2008). The IGM refers to the gas and plasma located in between galaxies; regions with huge ranges of temperatures where the densest regions are often less dense than the best vacuum humans have been able to create on Earth.

Approximately 30% of the current baryon census is thought to reside in the Warm-Hot Intergalactic Medium (WHIM; $T = 10^5$-10^7 K; Shull, Smith & Danforth 2012). The other large phase of the IGM is the Warm-Ionized Medium (or "Lyα forest"; $T = 10^{3.5} – 10^{4.5}$ K; Savage et al. 2014). The WHIM is of particular interest to the missing baryon problem because of how it has been incompletely studied in the past and thus may hold the key to finding the baryons. A more refined understanding of the WHIM could eventually lead to more accurate values for the size and baryon count of the WHIM which would help in "finding" some of these missing baryons.

1.2 The Intergalactic Medium

The most common way to observe the diffuse gas of the WHIM (and the IGM in general) is via the absorption lines in the spectra of distant Active Galactic Nuclei (AGNs). As light from the AGN travels toward Earth, it passes through different regions of gas (also called absorbers or systems). Based on the elements making up the cloud the spectral lines from the elements are absorbed out of the AGN's original spectrum leaving narrow absorption lines. These can be analyzed to find the parameters of the cloud, including its distance, column density, and potentially temperature.

The question then becomes which elements to use to observe the WHIM. Hydrogen is the most common element in the universe, which means we would normally use it to trace IGM gas. However, at WHIM temperatures, most of the hydrogen gas is completely ionized to HII (H^+) which cannot be detected because it has no bound electrons and thus has no atomic lines. Therefore, in order to trace the WHIM, other elements need to be used as proxies. In this study, oxygen will be used.

Oxygen is the most abundant metal in the universe ("metal" referring to an element heavier than hydrogen and helium) and it has many ionization states which are common at high temperatures. In particular, OVII (six-times ionized oxygen or O^{6+}) is the dominant oxygen ion in the WHIM temperature range. However, OVII's only atomic transitions are in the X-ray part of the spectrum and are thus very difficult to detect with the necessary resolution due to current telescope technologies. Instead of OVII, we will use OVI (five-times ionized oxygen or O^{5+}). OVI still covers a significant portion of the WHIM temperature range (it traces $T = 10^5 - 10^6$ K) and its transitions are in the ultraviolet (UV) which is easier to observe at high resolution and sensitivity than X-rays.

Other highly-ionized metal ions with similar ionization levels to OVI can also be used to trace WHIM gas in UV light. These include, but are not limited to, CIV (three-times ionized carbon) and NV (four-times ionized nitrogen). While these other elements could be used, OVI is the best choice due to its higher abundance, stronger atomic transitions, and higher peak temperature.

1.3 Ionization Mechanics

In the IGM, absorbers can become ionized by two possible processes. The gas can either be ionized due to photoionization (high energy photons) or collisional ionization (high temperatures). Photoionization occurs when high-energy light from stars or AGN reaches atoms in the IGM and is absorbed – transferring enough energy to one of the atom's electrons to allow it to escape the atom. Collisional ionization occurs due to thermal motion, and in the case of these IGM clouds, specifically motion caused by shocks. These shocks (material moving faster than the speed of sound) can be from galactic winds, cloud-on-cloud collisions, gravitational infall (Cen & Fang 2006), or supernovae. When shocks hit absorbers, collisions between atoms can be energetic enough to knock electrons off of atoms, thus ionizing them and heating the cloud.

From these definitions, it is clear that ions formed via photoionization do not indicate hot gas while ions from collisional ionization do indicate hot gas. However, it is possible for gas to initially be heated and ionized via collisional ionization but to then cool, resulting in cold, ionized gas not formed via photoionization. Non-equilibrium ionization, or "frozen-in" ionization, is this form of radiative cooling in which a cloud is initially ionized by collisional ionization, but then cools without the recombination of nuclei and electrons. This leads to an "over-ionized" gas – one which is ionized but no longer hot. This "recombination lag" can occur when clouds are at low enough densities to where their electrons are too far away from their nuclei to recombine (Gnat & Sternberg 2007).

1.4 Overview

In this study, we use data from the Cosmic Origins Spectrograph to determine the temperatures of IGM absorber systems. We then use these values to consider how these absorbers were ionized in order to determine which gas is part of the WHIM and which is not. These temperatures and other physical parameters of the clouds are also compared to determine if there are any correlations in the data. While

attempts to investigate the WHIM via this method have been made in the past, it has never been done with this large of a sample size before.

In Section 2, we outline the initial gathering and analysis of this data and then the specific methodology used to quantify and separate these systems. In Section 3, we discuss the analysis of these systems in terms of their physical parameters and the calculation of their temperatures. In Section 4, we detail the results of the different types of systems. Finally, in Section 5 we present a discussion in broader context, a summary of the study, and possible future work to be done.

2.0 Methods

2.1 Observations and Dataset

The data used in this study were taken using the Cosmic Origins Spectrograph (COS) attached to the Hubble Space Telescope (HST). COS was designed specifically to observe faint point sources in the UV and Far-UV (FUV) parts of the electromagnetic spectrum. In particular, it observes 1150-1800 Å in the FUV using two detectors – G130 (blue) and G160 (red) (Green et al. 2011).

This particular data set was compiled by Dr. Charles Danforth from archival COS data and consisted of 2611 absorption line systems along 82 AGN sight lines (Danforth et al. 2016). These sight lines were chosen in part due to their high signal/noise ratio which meant that they probed the IGM with good sensitivity to weak absorption. These sight lines also contained the entire Lyα forest which allowed the line identification to be more easily and unambiguously determined. Since this project's goal was to examine the nature of OVI in the IGM, only the individual absorbers detected in both HI and OVI from the original 2611 were included in this dataset. To identify the elements corresponding to these lines, first the Lyman series was identified wherever possible. Then, it was found whether or not the OVI doublet was present at approximately the same redshift as the Lyman series. This process led to 259 absorber systems along 52 sight lines in the range of $0.11 \leq z \leq 0.63$ identified as containing both HI and OVI absorption features which could then be analyzed more closely.

2.2 Absorber Profiles

We began our analysis of these spectra by creating best-fit curves for the spectral lines of interest – lines of HI and OVI which appeared close to the same redshift. Absorption lines are best modeled using

Voigt profiles which are a convolution of a Gaussian and a Lorentzian function. Gaussian curves represent the distribution of the velocities of individual particles in the cloud while Lorentzian curves characterize the quantum mechanical uncertainty in the energy change when a photon is absorbed/emitted in an atom. The properties of a cloud can be found from the shape of their absorption features because the Gaussian component of the feature depends on physical parameters (like temperature)

There are two main physical parameters that contribute to the Gaussian profile of an absorption line. The first is the Doppler b parameter (or b-value). This parameter is related to a standard deviation (σ) or a full-width half-maximum value (Γ) in that it is a way to measure the width of a Gaussian curve. b-values are used, rather than σ and Γ, in part because of tradition in the field. This parameter is also useful because it can be directly related to temperature. This relationship is shown in the equation below

$$\mathrm{T} = \frac{m b_T^2}{2k}$$

where b_T is the thermal component of the b-value (in km/s), m is the mass of the element who's b-value was used, k is Boltzmann's constant, and T is temperature (in K).

The other parameter is the column density of the cloud (measured in cm^{-2}) which is defined by the variable N and often referred to by $logN$. Due to the nature of how we discover these clouds, we cannot find their actual density. Since we do not know the line-of-sight depth of these clouds, instead, we find a two-dimensional (areal) number density. This is done by integrating three-dimensional space density n (cm^{-3}) over a path length l (cm):

$$N = \int n \, dl$$

However, it is important to note we also do not know the transverse dimensions of these clouds either since we only measure their parameters along the line-of-sight. Therefore, we are actually only measuring the density of one section of the cloud, and we are assuming that it is indicative of the integrated density of the entire cloud.

These *b* and *logN* values were chosen so that the Voigt profiles fit the spectral lines and the atomic parameters in question. From this fitting process, we were able to ascribe physical values to the plotted absorption lines which represent individual clouds of gas. Combining column density and b-value creates the fit of the Voigt profile, but the placement of these fits is also important. To place these profiles, the centroid of the absorption feature was found. This centroid wavelength (λ) can be related to the recessional velocity (*cz* or *v*) of the cloud via the equation

$$v = c\left(\frac{\lambda - \lambda_0}{\lambda_0}\right)$$

where λ_0 is the rest wavelength of the transition in question and *c* is the speed of light. The centroids of each of the Lyman series lines and OVI doublet features allowed us to find an overall recessional velocity for both HI and OVI. Then, finding the difference between the velocities of these elements gave us a velocity difference Δ*v*:

$$\Delta v = |v_{HI} - v_{OVI}|$$

Systems with large Δ*v* values (with HI and OVI moving at significantly different velocities) could mean several different things including that the HI and OVI features are not tracing the same cloud or that there is a shock front moving through the cloud creating a difference in velocity.

After finding the appropriate Voigt profile parameters (*v*, *b*, *N*) for the spectral lines, we plotted these Voigts over the normalized spectra. We began with a Python code created by Evan Tilton which was written to create single-component Voigt profiles and expanded on it to be able to plot an overall Voigt (seen in Figure 2.1 as the red curve) and individual Voigts (cyan curve). We then wrote code to create stackplots – the normalized spectra of different ions plotted on a common velocity scale – for each of our absorbers. Each stackplot contains 5 different plots of the absorption lines corresponding to HI and OVI at a specific redshift. These plots included the first three Lyman lines (at 1216, 1026, and 973 Å) and the OVI UV doublet at 1032 Å and 1038 Å. For systems at redshifts $z \geq 0.47$, the Lyα line is shifted out of the COS

spectrum and so for these cases we plotted Lyβ through δ (950 Å) rather than Lyα through γ. Example stackplots for two systems along the HE0153-4520 AGN sight line are shown in Figure 2.1.

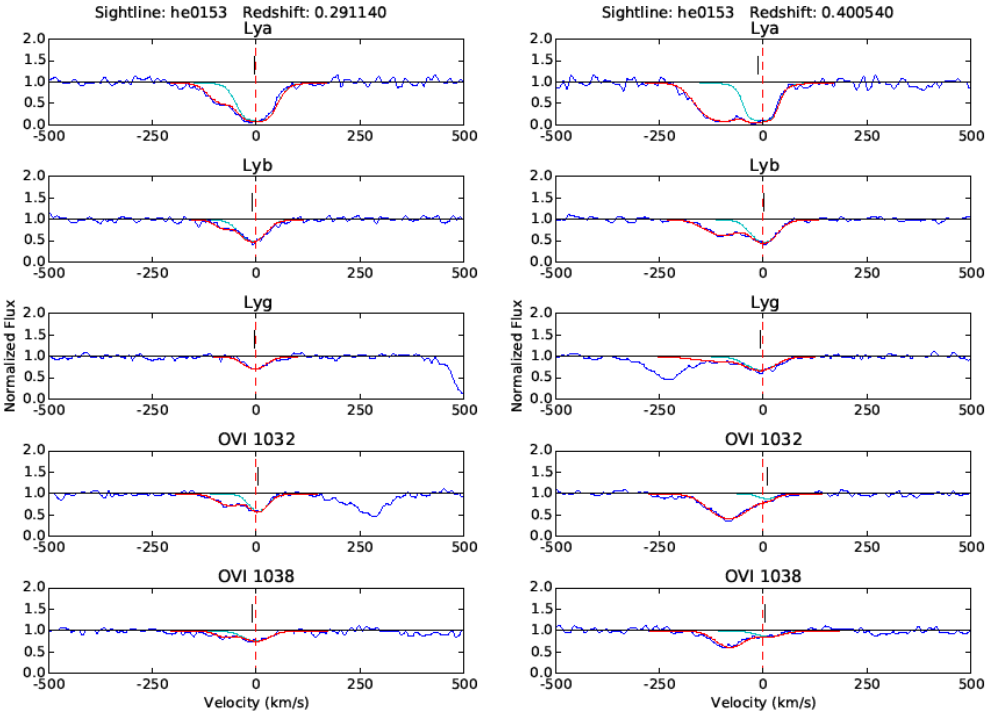

Figure 2.1: Two example stackplots are displayed with a vertical axis of normalized flux and a horizontal axis of v - v_{sys} in km/s (where $v_{sys} = cz$). The blue curve shows the AGN sight line data with the subtracted continuum, the red curve is a best fit Voigt for that element, and the cyan curve is the individual Voigt curve for the specific redshift. The vertical ticks mark the center of the Voigt curve. The dashed-red vertical line shows where the centroids of the lines would be if the elements were exactly aligned in velocity.

2.3 System Categorization

We separated the 259 systems into three categories: Aligned (Type 1), Non-Aligned (Type 2), and Ambiguous (Type 3). An Aligned system is one where the velocity of the HI in an absorber is very close to the velocity of the OVI in the same absorber (a small Δv value). This would mean that when a stackplot is created for the absorber, the centers of the HI and OVI features would line-up, one on top of the other (see the plots in Figure 2.1). A system that is Non-Aligned has a significant difference in the velocities of

the HI and OVI lines (a large Δv value), and an Ambiguous system is one that is too complex or has too many contributing factors to be able to categorize it as either Aligned or Non-Aligned beyond a reasonable doubt.

The importance of separating these systems comes from the desire to determine the systems' temperatures. Non-Aligned absorbers most likely have HI and OVI in different clouds or in different phases within a cloud, so each element has own temperature. On the other hand, absorbers with aligned HI and OVI have the possibility of the two elements being part of the same cloud which means that we can assign a temperature to the absorber using the two elements' absorption features (this methodology will be described in section 3.3).

Systems were classified as Aligned/Non-Aligned through a several step process. We first examined all of the stackplots of the systems. We found the velocity difference (Δv) between the HI and OVI lines and plotted them in a histogram. When using COS, the uncertainty of the velocity of ions in widely separated portions of the spectrum, like OVI and Lyα, can be fairly significant since they often fall in different parts of the detector. This can lead to systematic uncertainties often ranging from 10-20 km/s (Green et al. 2011). Thus, it is unrealistic to accept only systems with Δv = 0 km/s as aligned. Therefore, we used the 1σ cutoff of 68% as a way to quantitatively separate the Type 1s from the Type 2s. We found this value to be approximately Δv = 20 km/s. This allowed us to categorize most of the systems into either Type 1 or 2. These systems were then manually inspected to ensure that the categorization was reasonable. The histogram of Δv, with the systems separated, is shown in Figure 2.2.

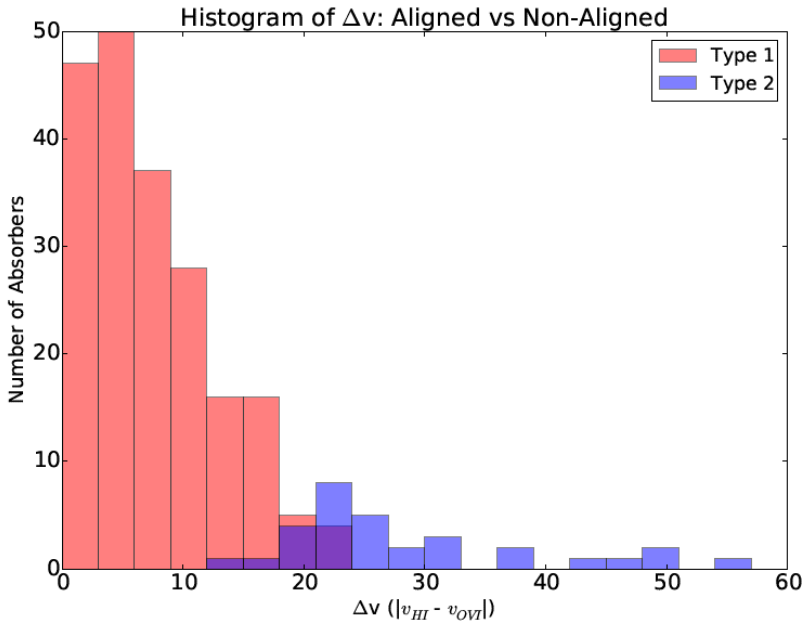

Figure 2.2: Histogram of the Δ*v* values (| $v_{HI} - v_{OVI}$ |) which shows the final Type 1s and 2s. There is some overlap in the histogram which is due to the classification of the Type 3s into the other two categories. These systems had more factors involved in their categorization than just Δ*v*.

However, having this cutoff value for Δ*v* was not a perfect system, specifically because it failed to take into account the Ambiguous (Type 3) systems. As these were re-analyzed and re-sorted, other factors came into play which made the histogram in Figure 2.2 have some overlap, rather than a distinct break between the two system types. The goal of the extra analysis of the Type 3 systems was to sort as many as possible into either the Type 1 or Type 2 categories, although some would remain ambiguous. Some of these systems were relatively easy to sort. Some systems needed to be completely removed because the HI or OVI lines detected were too weak to be interpreted as real, some systems needed just one of the individual lines removed due to a poor fit, and some systems needed to be re-fit completely.

Other Type 3 systems required more complex analysis. In some cases, we examined the alignment of HI with other metal ions of similar ionization level to OVI (for example, CIV). We also separated some multi-component systems into two different absorber systems. There were also nine systems which we

evaluated with detailed modeling. This was done for systems where one of the OVI features was well-fit by the Voigt model but the other was not. When doing this, we took the *logN* and b-value of the better-fit OVI line, applied it to the other OVI line, and then checked its fit. We could then ascribe the values of the single well-fit OVI line to the entire OVI feature. This method allowed us to check for consistency in the OVI profile and confirm the identification of the line as OVI.

This process of re-evaluating lines allowed many of the Ambiguous systems to be re-sorted into either Type 1 or Type 2. While placing Type 3s into the other two categorizes could lead to miss-categorizations, we do not believe they would have a large impact on the results of this study. This is because there were only ~20 systems which required complex analysis and most of these either remained Type 3s (and thus had no bearing on further analysis) or were re-classified as Types 1s (which had such a large sample size that any inaccurate categorizations would not deeply impact the dataset).

By the end of this categorization process, of the 259 HI-OVI systems that we began with, 203 were Type 1s, 31 were Type 2s, and 16 systems remained Ambiguous. Examples of each of these types can be found in Figure 2.3. After this re-evaluation process, most of the lines that were still determined to be ambiguous were due to one of two reasons. First, the HI or OVI lines were blended with other absorption features to the point where they could not be dis-entangled or second, the HI lines in the system were too saturated to be able to identify the number of components that were actually present. An example of an Ambiguous system is shown in Figure 2.3.

Type 1: Aligned Systems:

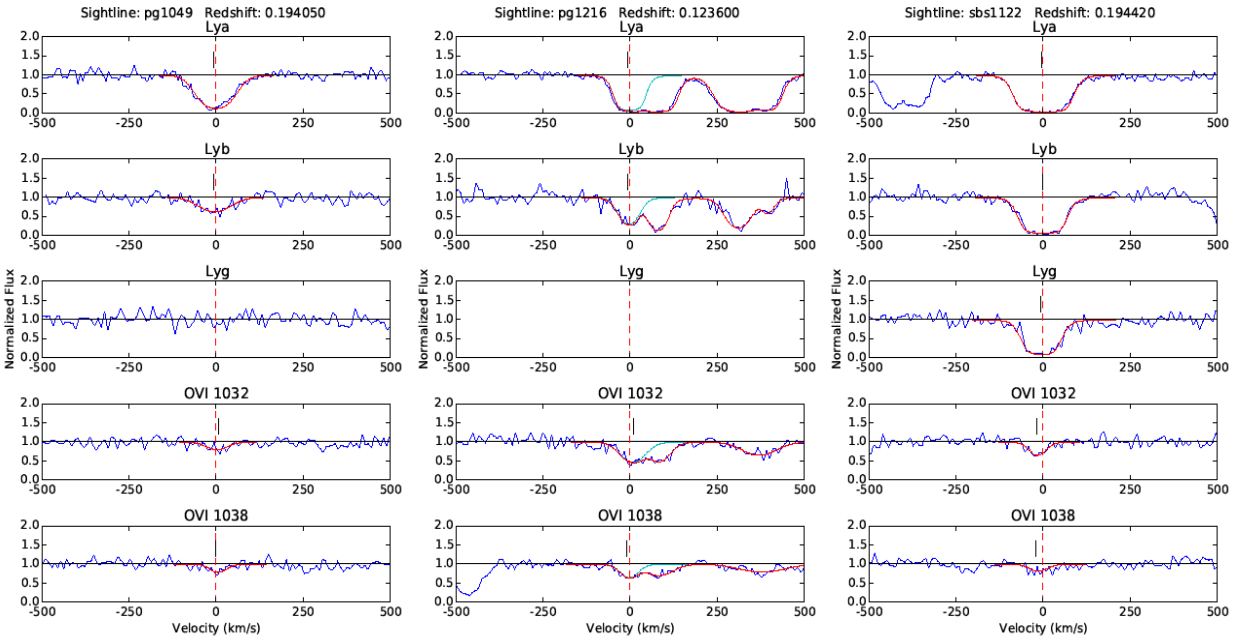

Type 2: Non-Aligned Systems:

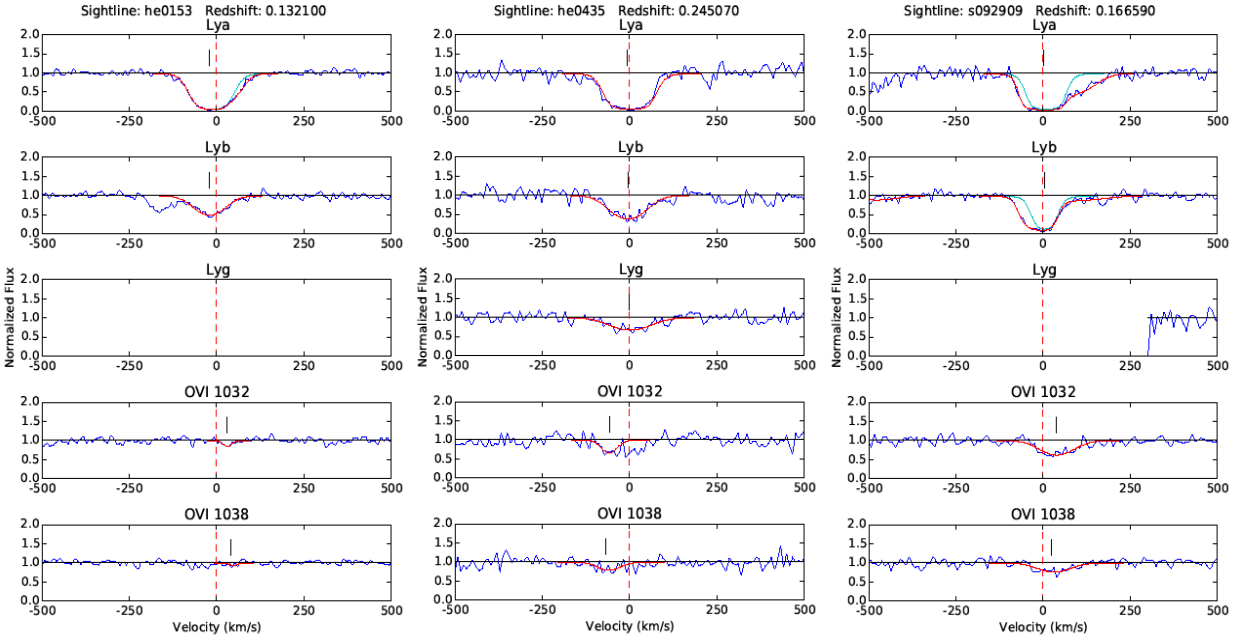

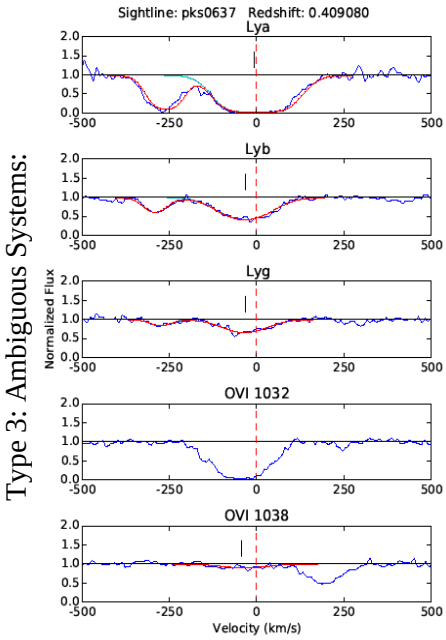

Figure 2.3: Seven stackplots for OVI and HI systems which serve as examples for the three different categories for the original 259 absorber systems. The first three plots show examples of Aligned systems. The second row of plots shows examples of the Non-Aligned systems (note how there is an offset between the centroids of the HI and OVI absorption features). The final plot shows an example of an Ambiguous system. This system in particular was deemed ambiguous due to the fact that HI is broad and saturated to the point where it could contain multiple components along with the fact that the stronger 1032 Å line is blended and the weaker 1038 Å line is so small.

3.0 Analysis

3.1 Doppler Parameters

All absorber systems have two different Doppler parameters ("b-values") to consider. They have one that describes the HI absorption features and one that describes the OVI absorption features. This is true for both the Type 1 and Type 2 systems.

The b-values for each of the individual absorption features were originally found in Danforth et al. (2016) and were then re-measured as necessary to ensure an accurate fit. Since there are multiple absorption features for each ion (two for the OVI doublet and up to ten for the Lyman series, although usually ≤ 4 were used), these values had to be combined in order to gain an overall Doppler parameter for each of the ions. This was done using different methods for the HI and OVI lines. For OVI, the overall b-value was found with an average of b-values from the individual lines. This was true except in cases where one of the lines was omitted when it was too weak or appeared blended with other absorption features. In these situations, the b-value of the unblended OVI doublet line was used for the overall OVI b-value.

While this was the best way to find the b-values and column densities for the OVI absorbers, better measurements for both HI's *b* and *logN* values were found with a curve of growth (CoG) solution. CoGs describe how the equivalent width of a Voigt profile grows as the column density increases. This method was used for Lyman lines that were saturated to the point where there could be multiple absorbers components hidden within the curve. In this case, one option would be to only use the lower-level, non-saturated Lyman lines and simply ignore the saturated lines. However, this would mean throwing away data when it wasn't necessary. The curve of growth technique allowed all the data to be used to find the most accurate *b* and *logN* values for the system. This process consisted of plotting each of the Lyman lines on an

Equivalent Width vs Column Density (N) * Oscillator Strength (f) * Rest Wavelength (λ) graph and finding the best fit curve to match the data.

While the CoG technique is useful for HI features, it is not applied to OVI for two reasons. The first is that it is very rare to see saturated OVI lines and thus the curve of growth function is not necessary – b and $logN$ values can be determined reasonably accurately from the best-fit Voigt profiles alone. The other reason is that the f-λ contrast is extremely low for OVI and there are only two measured transitions, meaning that these two data points would be very close together on the curve of growth, and thus no conclusive best fit line could be found. These CoG HI and averaged OVI b-values were then plotted to show their range and distribution (see Figure 3.1).

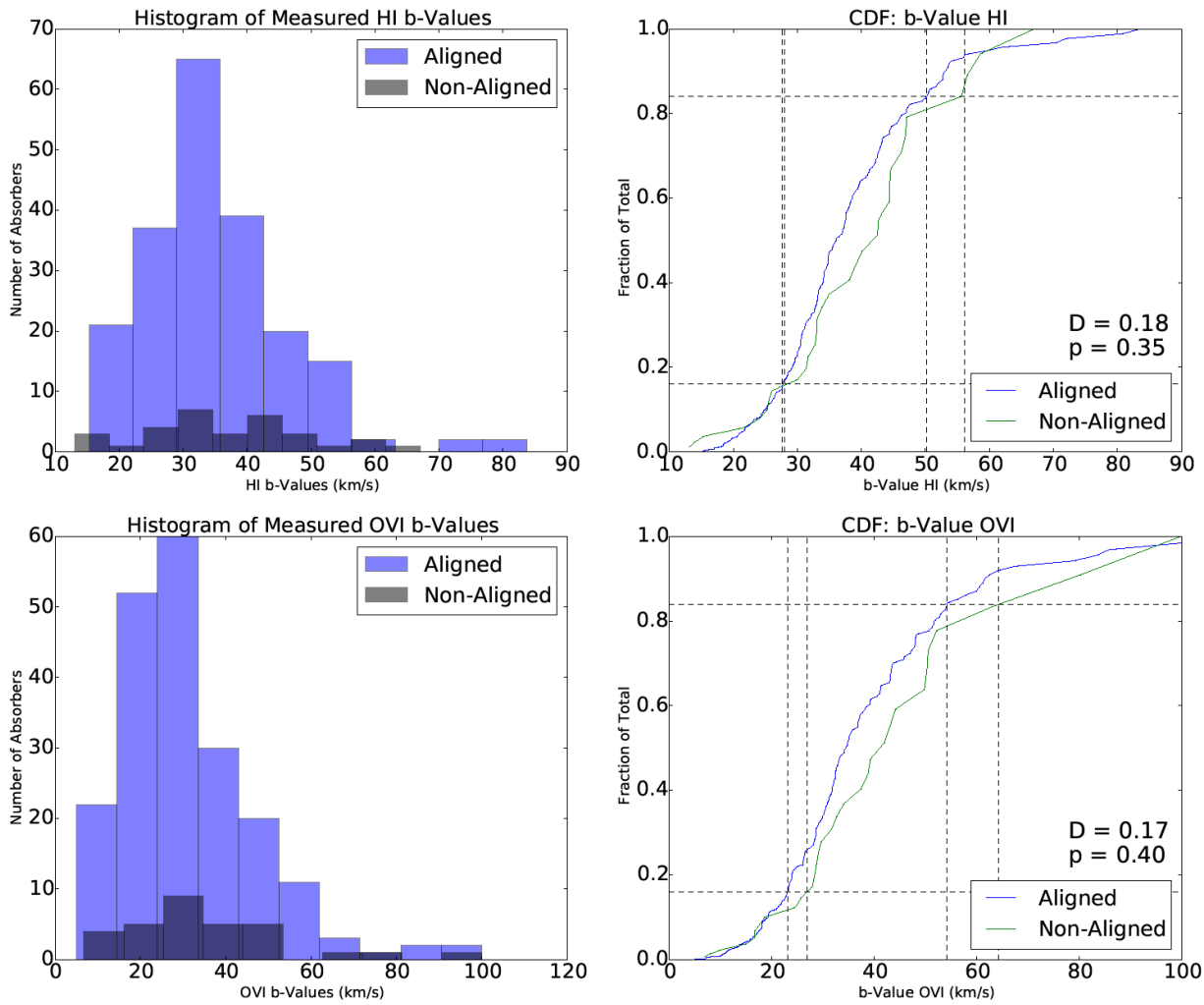

Figure 3.1: Histograms and Cumulative Distribution Functions (CDFs) for the HI and OVI Doppler Parameters. They include data from both the Type 1 and Type 2 systems. The dashed lines on the CDF plots allow for easy identification of the 1σ points in the data. The D and p values for these systems is also include on the CDF plots.

The Cumulative Distribution Functions (CDFs) in Figure 3.1 show that the Aligned and Non-Aligned systems have significantly different distributions of b-values. Specifically, the Non-Aligned systems have measured b-values that are larger than the Aligned systems, both when considering the HI and OVI b-values. The significance of this difference can be measured using a statistical Kolmogorov-Smirnov (K-S) test. After applying this test, it was found that the HI b-values of the Type 1 / 2 sample have

a D statistic of 0.175 and the OVI b-values have a D statistic of 0.168. These D statistics represent the absolute maximum vertical distance (supremum) between the CDFs of the two samples, and therefore these values show that there is a notable difference between the Type 1 and 2 systems' b-values. These D statistics also correspond to p-values of 0.35 and 0.40 for HI and OVI respectively. In both cases, these p-values show that there is no way to say that the Type 1 and 2 systems are distinct in this regard.

3.2 Column Density

The other measured quantity for these systems is the column density of the gas. Just as with the Doppler parameters, the column density of the individual absorbers were taken from Danforth et al. (2016), re-measured as necessary, and then $logN_{HI}$ was found via CoG solutions while $logN_{OVI}$ was found by averaging the *logN* values of the two OVI lines. This process followed the same reasoning as described for the Doppler parameters.

The column densities of these systems range from $logN_{HI} = 12.6 – 17.1$ and $logN_{OVI} = 12.9 – 14.9$. These values align with the results found by Tripp et al. (2008), Savage et al. (2014), and Danforth & Shull (2005) all of which found approximately $logN_{HI} \sim 12.5 – 16.0$ and $logN_{OVI} \sim 13.0 – 14.5$. However, this study finding a larger range makes sense since this sample is larger than the previous studies and a larger sample size would lead to a higher probability of finding an outlier. When this data is plotted in a CDF, it shows that the column densities for the Type 1 and 2 systems are nearly identical when observing an individual ion (see Figure 3.2).

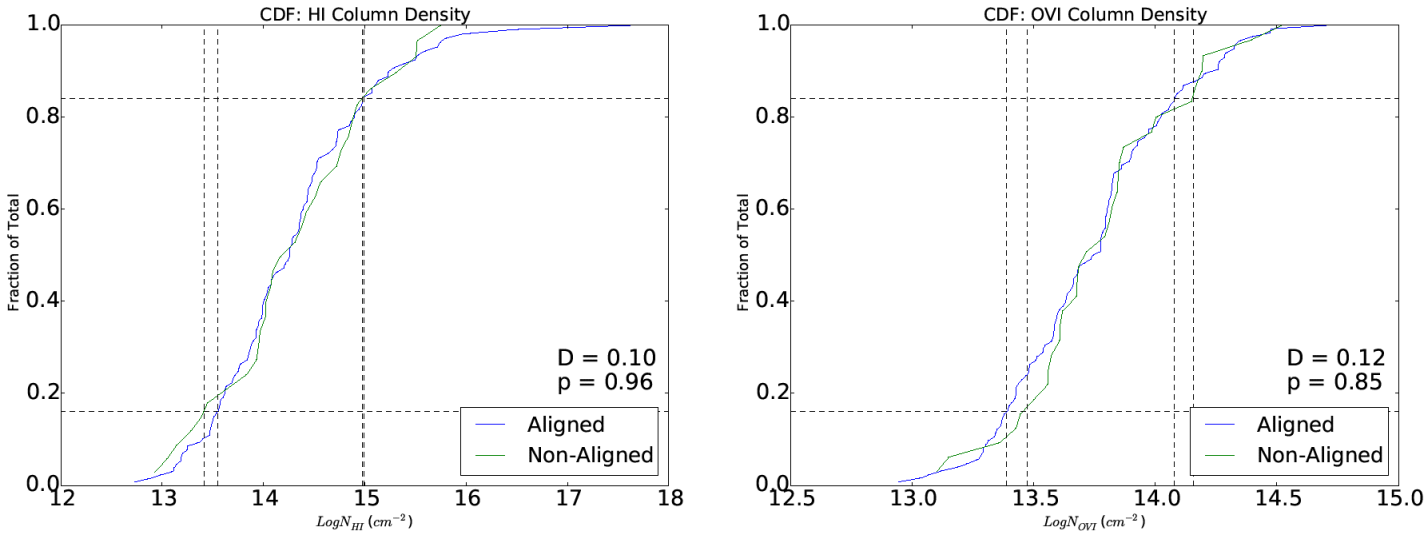

Figure 3.2: Cumulative Distribution Functions for the column density of HI and OVI absorption features. The data for the Type 1 (Aligned) and Type 2 (Non-Aligned) data is over plotted. The dashed lines allow for easy identification of the 1σ points in the data. The D and p values for these systems is also included on the plot.

These distributions have K-S tests resulting in D statistics of 0.098 for HI and 0.120 for OVI which show that there is very little difference between the Type 1 and 2 *logN* distributions. The K-S test also resulted in p-values of 0.96 for HI and 0.85 for OVI which indicate that there is no way to say whether these two distributions are derived from the same parent distribution. Through Figure 3.3 it can also be seen that there is no evidence of correlation between the OVI and HI column densities. This lack of correlation is consistent with many previous works (e.g. Savage et al. (2014), Danforth & Shull (2005), and Danforth et al. (2016)). However, unlike these pervious works, this plot has the Aligned and Non-Aligned systems separated which shows that this lack of correlation is equally present in both these types of systems.

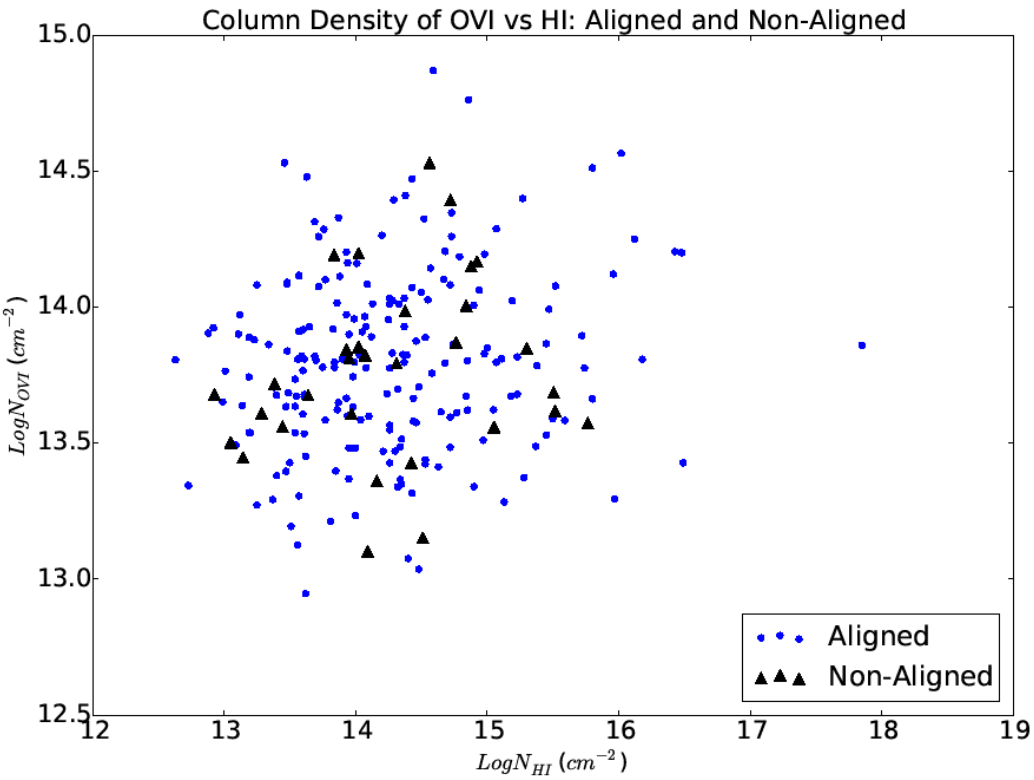

Figure 3.3: Plot comparing the HI and OVI column densities of the absorbers, specifically with the Aligned and Non-Aligned systems separated.

3.3 Calculation of Temperatures

The ultimate goal of this project was to be able to obtain the temperatures of IGM gas clouds. This can be done by using the determined HI and OVI b-values of the systems since they are partially a function of temperature. The b-values that are found from Voigt profiles are a combination of thermal and non-thermal components related by the equation:

$$b^2 = b_T^2 + b_{NT}^2 \tag{1}$$

where b_T is the thermal component of the b-value and b_{NT} is the non-thermal component. The thermal component of the b-value refers to the microscopic motions of individual atoms while the non-thermal b-value relates to the macroscopic bulk motion and turbulence inside of the cloud. Therefore, for systems

with aligned HI and OVI (Type 1s), the non-thermal b-value for HI and OVI should be identical since the gas is presumably in the same cloud.

$$b_{NT,HI} = b_{NT,OVI} \tag{2}$$

The thermal components of the b-value for HI and OVI are also related. By taking a ratio of HI and OVI in the equation:

$$T = \frac{mb_T^2}{2k} \tag{3}$$

and assuming they have the same temperature (so $T_{HI} / T_{OVI} = 1$), it is found that $b_{T,HI}$ and $b_{T,OVI}$ are related by the square root of the ratio of their element's masses, which is logical since heavier atoms will move more slowly at a given temperature. Since oxygen has an atomic weight of 16, oxygen atoms move four times slower than hydrogen atoms at the same temperature:

$$b_{T,HI} = 4 * b_{T,OVI} \tag{4}$$

Equations 1, 2, and 4 can be solved to find the three different components of the b-values of the system, $b_{T,HI}$, $b_{T,OVI}$, and b_{NT}:

$$b_{HI,T}^2 = \frac{1}{15}(b_{HI}^2 - b_{OVI}^2) \tag{5}$$

$$b_{OVI,T}^2 = \frac{16}{15}(b_{HI}^2 - b_{OVI}^2) \tag{6}$$

$$b_{NT}^2 = \frac{1}{15}(16 * b_{OVI}^2 - b_{HI}^2) \tag{7}$$

Then either of the thermal b-values can be substituted into equation 3. However for simplicity, assuming that T is in Kelvin and b_T is in km/s, we can combine the constants in equation 3 and instead use:

$$T = A * \left(\frac{b_T}{0.129}\right)^2 \tag{8}$$

where A is the atomic number of the element used for the thermal b-value.

By examining equations 5-7 it can be seen that a value for b_T (either HI or OVI) and b_{NT} can be found only if the total b-values relate such that $b_{HI}^2 > b_{OVI}^2$. However, this is not always the case. While hydrogen normally has larger b-values than metals, b_{HI}^2 could be greater than b_{OVI}^2 if the HI and OVI are in fact part of different clouds (and just moving at the same velocity) or if the lines actually have more components or are blended. From this, the Type 1 systems were sub-divided into two sub-categories: Type 1a and 1b. Type 1a's were the 118 systems of the original 203 which had $b_{HI}^2 > b_{OVI}^2$ and could therefore have their accurate (within uncertainties) temperature determined via equation 8. Type 1b's on the other hand were the 85 systems which had $b_{HI}^2 < b_{OVI}^2$ and therefore could not have an accurate temperature found.

3.4 Uncertainties

The initial data from Danforth et al. (2016) provided uncertainties for the *b* and *logN* values. While it was possible to formally follow propagation of uncertainties to find errors for this study's computed values (b_T, b_{NT}, and temperature) this was not the simplest, nor the most useful method. Instead, we chose to find empirical uncertainties for these values in order to avoid complications due to any correlation between b_{HI} and b_{OVI} and also to keep the values rooted in observational data.

To find these empirical uncertainties for both the b-values and temperature, we looked at how the output value would change if the inputs were varied by their uncertainties. Specifically for the temperature uncertainties, we could write temperature as a function of b_{HI} and b_{OVI} (its input factors) – $T(b_{HI}, b_{OVI})$. Therefore, to find the possible maximum and minimum values for the temperatures of Type 1a systems, we found $T(b_{HI} + \delta b_{HI}, b_{OVI})$, $T(b_{HI} - \delta b_{HI}, b_{OVI})$, $T(b_{HI}, b_{OVI} + \delta b_{OVI})$, and $T(b_{HI}, b_{OVI} - \delta b_{OVI})$. Then largest and smallest of these four values were used as the uncertainty range for the output value. However, in certain cases, it was not possible to find a finite result for these values which led to only one limit on the temperature.

This method was also used to find a temperature range for the Type 1b systems, since their accurate temperatures could not be calculated. This was again done by varying the temperature inputs, this time by $\pm 1\sigma$, and seeing if they would yield a finite result. This ended with the four possible outputs: $b_{HI} \pm \sigma_{\mathrm{HI}}$ and $b_{OVI} \pm \sigma_{\mathrm{OVI}}$. Then, the maximum and minimum of these four values were taken to be the temperature range.

This method did not work for all of the Type 1b systems – some had b-values such that even changing them by 1σ was not enough to make $b_{HI}^2 > b_{OVI}^2$. However, this was enough for many of the systems. From this method, we found an upper and lower limit on the temperature for 19 of the 85 Type 1b systems and at least one limit on 17 other systems.

4.0 Results

4.1 Overall Results

Considering both the Type 1 and Type 2 systems, several measured quantities were plotted to look for any correlations. These included the column density vs. the measured b-value of the system and Δv vs b-value (both HI and OVI). Figure 4.1 shows that there is no evidence that the parameters (N, b, and Δv) of the absorber systems are correlated. Therefore, they are most likely all physically independent from one another.

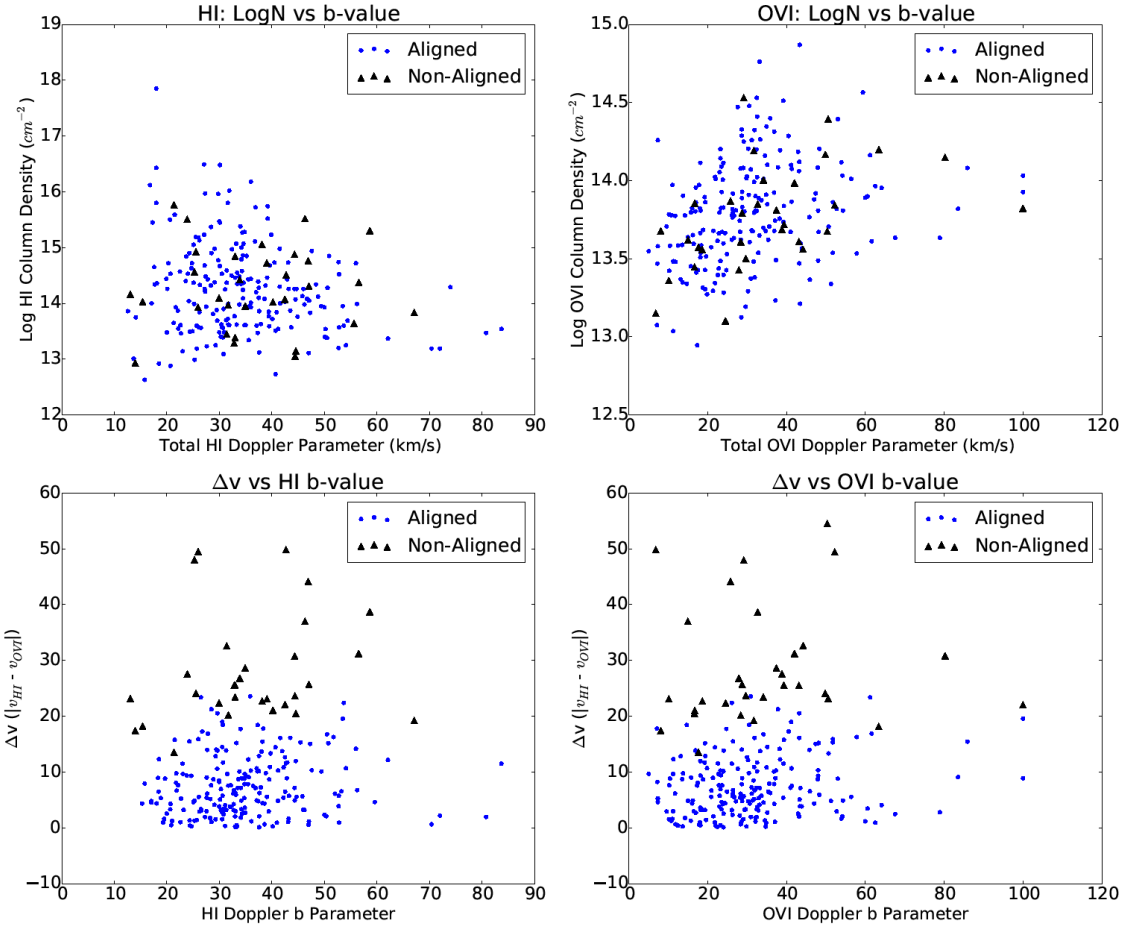

Figure 4.1: Plots of different measured quantities: The top two are column densities vs b-values for HI and OVI. The bottom two are Δv vs b-values. Since the types of systems are defined by their Δv value, these will obviously be different between Type 1 / 2.

4.2 Aligned System Results

4.2.1 Temperature Results

Using the methods outlined in Section 3.3, the temperatures of the Aligned systems were calculated. This resulted in a distribution of temperatures shown in Figure 4.2. The Aligned systems have a skewed distribution of their temperatures with a median value of $logT$ = 4.65 (T = 45,000 K) and a ±1σ range of 4.22 – 5.03 (17,000 – 107,000 K).

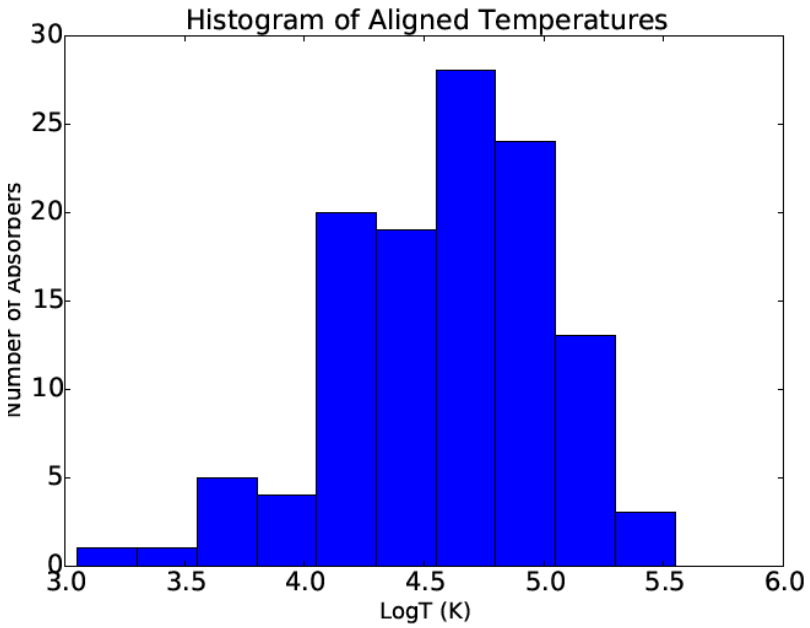

Figure 4.2: Histogram showing the temperature distribution of the 118 Type 1a (Aligned) systems determined via Equation 8.

To gain more insight, this temperature data was plotted against column density in Figure 4.3. This has been attempted in studies like Stocke et al. (2014) and Savage et al. (2014), but neither had large enough data samples to find a statistical result.

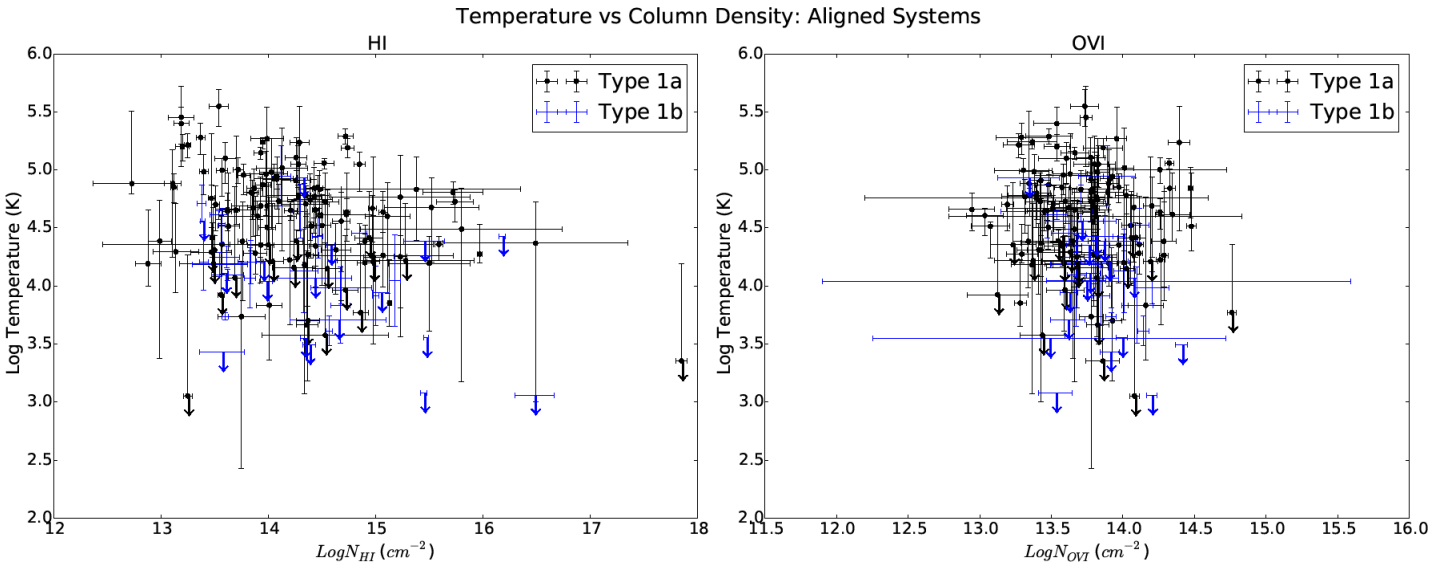

Figure 4.3: The relationship between the temperature and column density (both HI and OVI) for Type 1 systems (both Type 1a and 1b). Arrows are used when error bounds could not be computed.

Figure 4.3 shows that, for Aligned systems, temperature is probably not correlated with the column density of either ion. Temperature and column density should have some correlation, however there are many parameters involved in this relationship (including ionization fraction and total hydrogen column density) that we simply do not know. Therefore, most likely the correlation is lost within these unknowns.

4.2.2 Non-Thermal Doppler Parameter Results

The other quantity found by solving the equations from Section 3.3 was b_{NT} (equation 7). Since HI and OVI are assumed to be co-spatial (mixed) in the Type 1 systems, these elements have the same b_{NT} value. Figure 4.4 shows the distribution of the b_{NT} values for the Aligned systems.

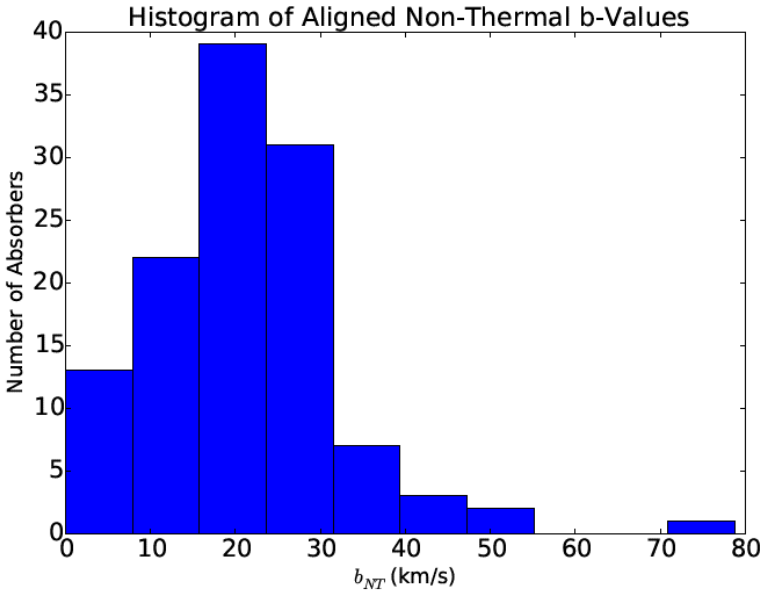

Figure 4.4: Histogram of the non-thermal Doppler parameters for the Type 1 (Aligned) Systems.

This skewed distribution has a median value of b_{NT} = 22 km/s and ±1σ range of 17 – 34 km/s. This provides us with an idea of the bulk velocities within IGM clouds. This value seems appropriate since our value is on the same order as the typical Interstellar Medium (ISM) sound velocity of ~10-20 km/s. These b_{NT} values were then compared with the temperatures of the Aligned systems in Figure 4.5.

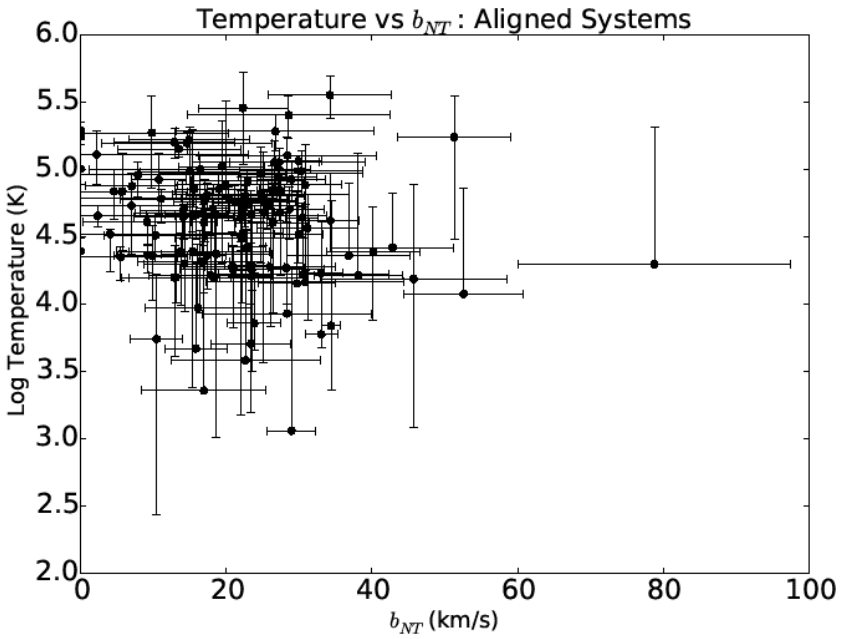

Figure 4.5: The relationship between the temperature of the aligned systems and their non-thermal b values.

Figure 4.5 shows a lack of correlation between b_{NT} and temperature (and thus b_{NT} and b_T) in the Type 1 systems (R = -0.17). There also appears to be no correlation present between b_{NT} and *logN* (with R = -0.037 and R = 0.308 for $logN_{HI}$ and $logN_{OVI}$ respectively). These values show that there is probably no correlation between HI column density and b_{NT} and while the correlation is higher for OVI column density and b_{NT}, it is still weak. The results of this section show that none of these other measured parameters correlate with the temperature of the Type 1 systems.

4.3 Non-Aligned System Results

4.3.1 Method for Determining Statistical Temperature

For the Aligned systems, it was possible to determine both b_T and b_{NT} for the clouds, but the same was not true for the Type 2 systems since their lack of velocity alignment meant that their clouds are at

different velocities and thus are not co-spatial. Therefore, the non-thermal b-values could not be assumed to be identical for HI and OVI in these Type 2 systems (equation 2 does not hold). This means that the system of equations presented in Section 3.3 could not be solved and thus it was impossible to directly calculate a temperature for these clouds.

However, there was another way to find a statistical, inferred temperature for these systems. In order to use the equations and method from the Type 1 systems (and outlined in Section 3.3), a b_{NT} value would need to be assumed for the Type 2 systems. The b_{NT} distribution for the Type 1 systems provides some guidance in terms of these values, but it could only be applied directly to the Type 2 systems if two cases were met. First, there had to appear to be no physical differences between Type 1 and 2 clouds so that they would logically have the same or similar b_{NT} distributions. Second, b_{NT} could not correlate with any of the other parameters so that even if the two types of systems were physically different, it would not impact their b_{NT} values.

In this case, there was no difference between the column density distributions of the Type 1 and 2 systems (Figure 3.2). While there was a difference between the b-values (Figure 3.1), this can be attributed to the two types of systems having different temperatures ranges (so different b_T values). Also, the graphs in Section 4.2 show that there was no correlation between b_{NT} and any other physical parameters of the Type 1 clouds. This can be seen in the plots of temperature vs b_{NT} (Figure 4.5) and temperature vs $logN_{HI\ or\ OVI}$ (Figure 4.3) which therefore implies no correlation between b_{NT} and $logN_{HI\ or\ OVI}$. Therefore, because we saw no differences in the physical parameters of the Type 1 and 2 systems and saw no correlations of b_{NT} with the other Type 1 parameters, we could reasonably expect a similar distribution of b_{NT} for the Type 2s to what we saw for the Type 1s. These results mean that the method outlined above was possible.

The next step was to use this distribution in a way that resulted in a single b_{NT} value which could be applied to the Type 2 systems. Due to the skewed nature of the Type 1 b_{NT} histogram (Figure 4.4), the median (rather than the average) b_{NT} value was found from the Type 1 data. This $b_{NT,\ med}$ was found to be 22 km/s and was then combined with the measured b-values for all the Non-Aligned systems using the

equations in Section 3.3 in order to produce an "inferred temperature" for each of the Type 2 systems. To provide a limit on this inferred temperature data, the maximum possible temperature for these Non-Aligned systems was also found by calculating the temperatures assuming that $b_{NT} = 0$, since this would assume all of the velocity inside the cloud was thermal.

Something important to note is that while this method does not accurately produce temperatures on a system by system basis, it does produce a logical estimate for the distribution of temperatures for the entirety of the Type 2 systems under the assumption that the distribution of b_{NT} is the same for the Type 1 / 2 absorbers.

4.3.2 Temperature Results

This method of determining inferred temperatures was used to produce four temperatures for each Type 2 system: $b_{NT} = 0$; for both HI and OVI and $b_{NT} = 22$ km/s; for both HI and OVI. The distributions of these inferred temperatures are shown in Figure 4.6.

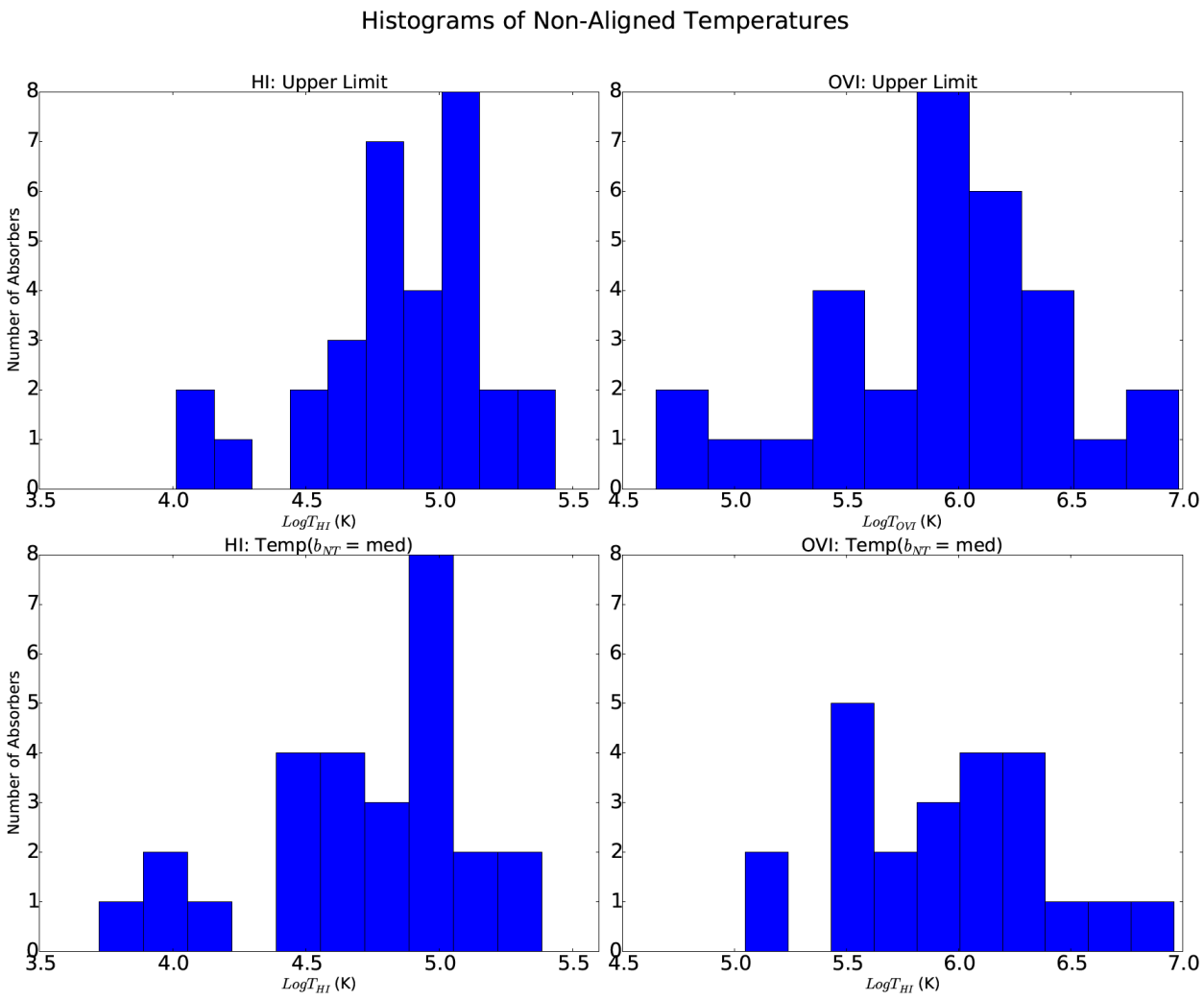

Figure 4.6: Histograms of the inferred temperatures of the Type 2 (Non-Aligned) systems. The top two histograms were found assuming b_{NT} = 0. The bottom two histograms were found assuming that the median b_{NT} value for the aligned systems of 22 km/s could be applied to the Non-Aligned systems as well. The upper and median histograms for the two elements do not have equal numbers of values because of the mathematical limits on calculating the median temperatures.

These distributions have median values and ±1σ ranges of: $logT_{HI,upper}$ = 4.87 (with a range of 4.56 – 5.13), $logT_{HI,med}$ = 4.80 (with a range of 4.44 – 5.11), $logT_{OVI,upper}$ = 5.98 (with a range of 5.42 – 6.38), and $logT_{OVI,med}$ = 5.99 (with a range of 5.50 – 6.31). In order to understand the relationships between these inferred temperatures and other physical parameters, temperature was plotted against the Δv values of the systems (the difference in velocity between HI and OVI; Figure 4.7) and the column density of the clouds

(both HI and OVI; Figure 4.8). Finally, these inferred HI and OVI temperatures were plotted against one another (Figure 4.9).

In these three figures, when an error could not be calculated, the error bars on the inferred temperatures were replaced by an arrow. Inferred temperatures also could not always be calculated which explains why the plots in Figures 4.7 – 4.9 have different numbers of data points. These calculations were made impossible when the observed width of the absorption features were narrower than the non-thermal value we were assuming (when $b_{total}^2 < b_{NT}^2$). It can also be seen that the errors for the HI and OVI temperatures are constant across all the data. This is due to the statistical methods of determining uncertainties in which the b_{NT} uncertainty is uniform for all absorbers. Together these plots show that there is no correlation between the inferred temperatures and any of these physical parameters for the Type 2 systems.

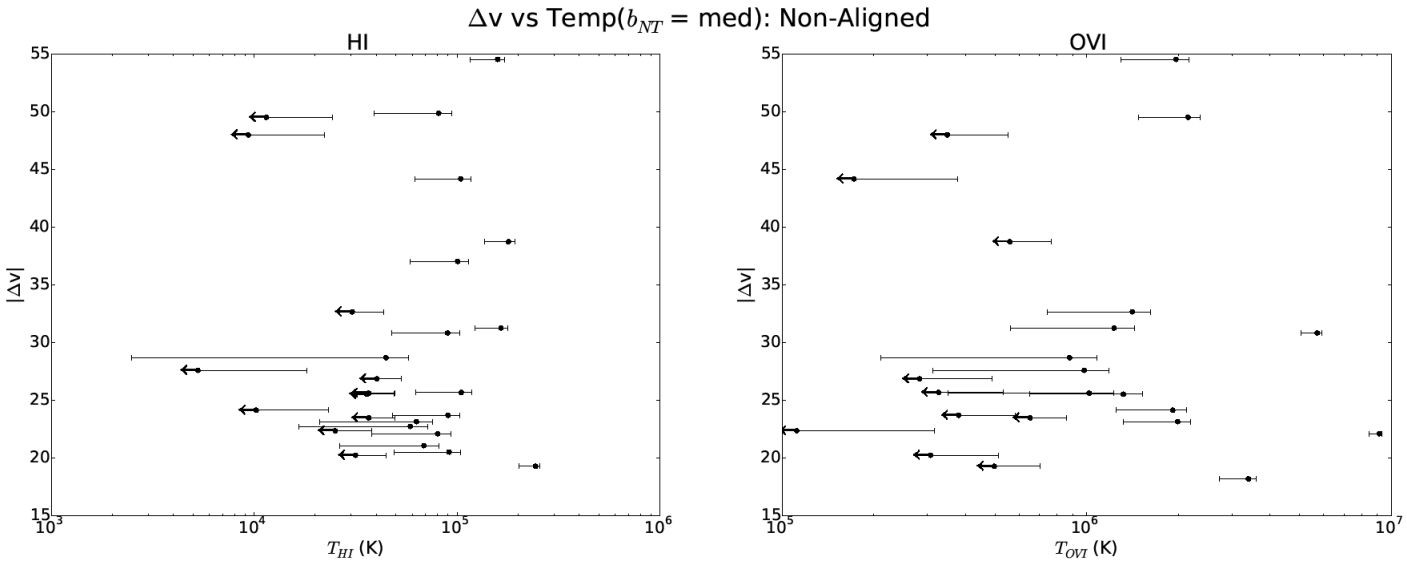

Figure 4.7: The velocity difference between HI and OVI plotted against the HI/OVI inferred temperature.

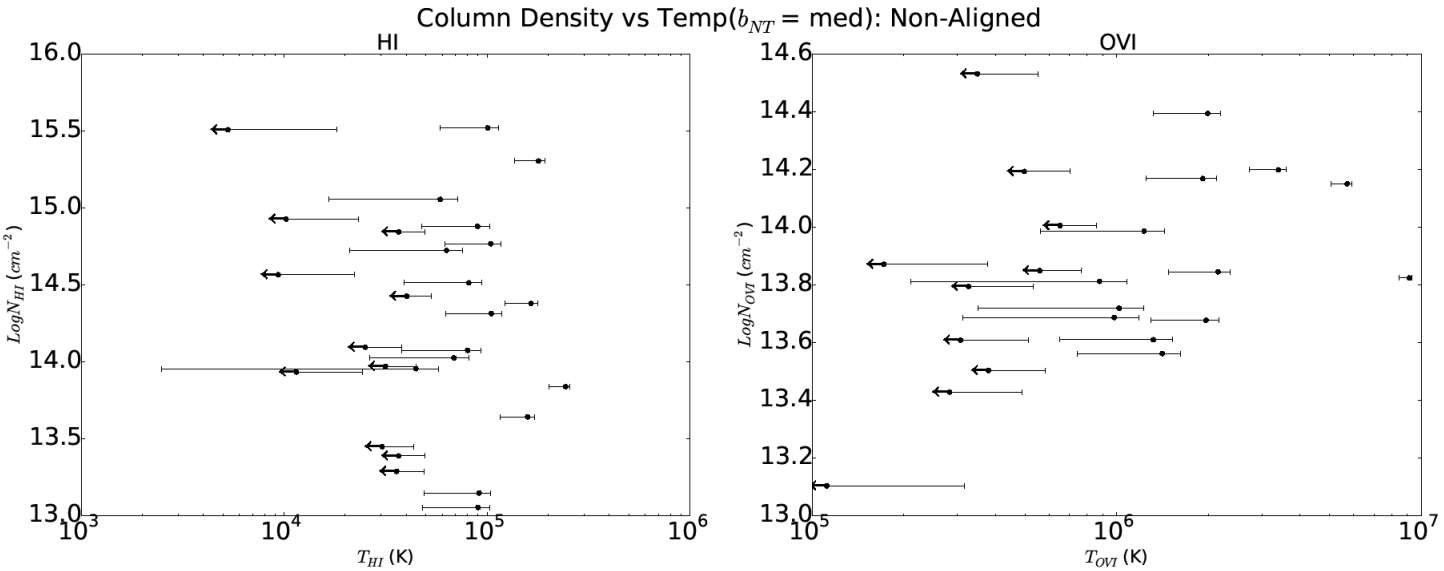

Figure 4.8: Relationship between the HI/OVI temperature of the system and their respective HI/OVI column densities.

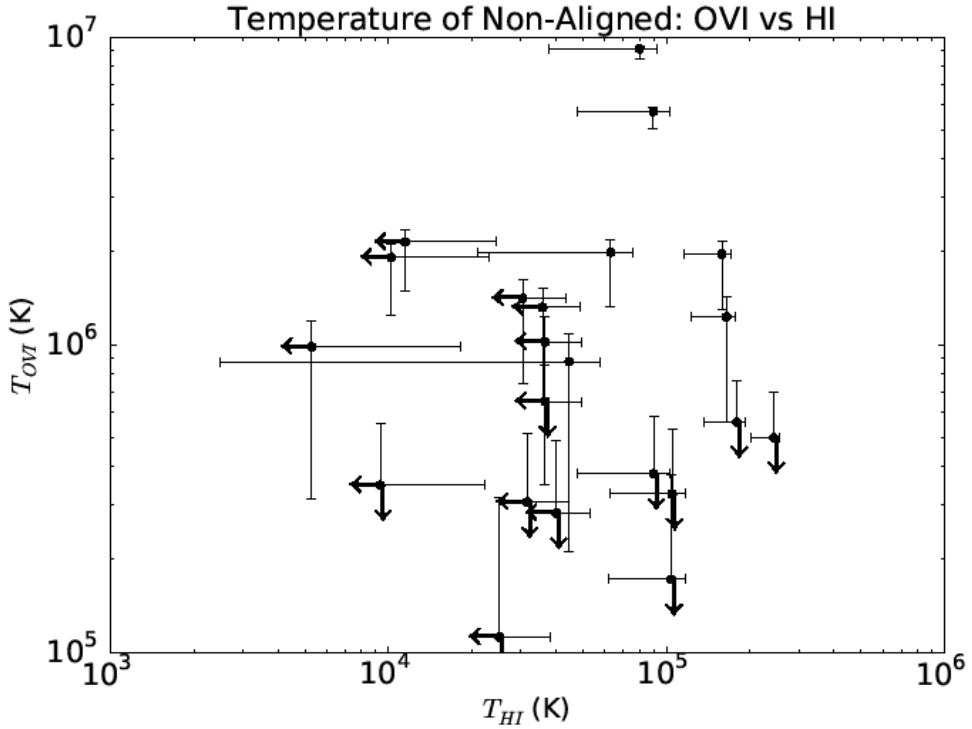

Figure 4.9: HI and OVI temperatures of the Type 2 systems plotted against each other.

5.0 Discussion and Conclusion

5.1 Discussion

This study of IGM absorber systems led to two major results that require further analysis: the calculated temperatures of the Type 1 (Aligned) systems and the inferred temperatures of the Type 2 (Non-Aligned) systems.

We found a temperature range of $logT$ = 3.05 – 5.55 for the Aligned systems (see Figure 4.1). This is lower than what would be expected for collisionally-ionized OVI. In collisional ionization equilibrium (CIE), the OVI fractional abundance peaks at $logT$ ~ 5.45 (or ~300,000 K; Sutherland & Dopita 1993) with a significant fraction between 5 < $logT$ < 6. This is not the distribution found in this study since the Aligned systems have $logT_{med}$ = 4.65. However, our result is consistent with the Tripp et al. (2008) and Savage et al. (2014) which found the average temperature for well-aligned systems was $logT_{avg}$ = 4.42 and $logT_{avg}$ = 4.78 respectively. Stocke et al. (2014) found an average temperature of $logT_{avg}$ = 5.12, but in this case there was a mixture of aligned and non-aligned systems.

The low temperatures of these Aligned systems most likely indicate that they were not shock heated and thus are not part of the WHIM phase of the IGM. This leaves two major possibilities. The first is that the clouds could have be photoionized by high-energy photons. Ionizing oxygen to OVI requires photons of 113 eV (λ ≤ 106 Å; or soft x-rays). Such high energies mean that a high ionization parameter (U; the density of ionizing photons relative to atoms) is required:

$$U = \frac{n_{photon}}{n_H}$$

which depends on n_{photon}, the density of ionizing (≥ 113 eV) photons, and n_H, the density of atoms. We currently do not have much information on such a high energy ionizing background, but almost all models

show that the density of high-energy photons is small (Haehnelt et al. 2001, Haardt & Madau 2012). Therefore, the only way to produce a high ionization parameter is to decrease n_H. This would require huge clouds (on the order of Mpc across) in order to provide the observed column densities. However, OVI is normally correlated with galaxies and a typical galaxy halo is only ~200 kpc in radius. Clouds on the order of Mpc would go against the current understanding of galactic feedback. Therefore, it appears that finding a situation when photoionization is common requires rethinking our understanding of extragalactic environments.

The second possibility for this low temperature result is that the cloud could have been originally shock heated but then cooled over time. If the cloud were low enough density, then the ionized nuclei and their free electrons would be too far apart to efficiently re-combine as the gas cooled. This process is known as non-equilibrium ionization and would result in a cool but ionized gas cloud (Gnat & Sternberg 2007). The aligned system temperatures found in this study are still too cool to match non-equilibrium ionization models, but they agree more with these models than they are to the models of collisional ionization. It is most likely that a combination of photoionization and non-equilibrium ionization is responsible for the low temperatures of these Type 1 systems.

The temperature range of the Type 2 (Non-Aligned) systems is also an interesting result. According to the distributions plotted in Figure 4.6, the average inferred temperatures were found to be $logT_{HI,med}$ = 4.80 and $logT_{OVI,med}$ = 5.99. Logically, the HI temperatures are much less than the OVI temperatures. However, more interestingly the OVI is hot – significantly hotter than the temperatures calculated for the Type 1 systems – thus making these systems likely part of the WHIM. However, this inferred temperature range is *higher* than the range expected for CIE: peaking near $logT_{OVI,peak}$ = 6.0. Since these temperatures are inferred rather than directly calculated, this does not necessarily mean that these Non-Aligned systems are not collisionally ionized. These Non-Aligned systems have temperatures closer to what would be present due to collisional ionization, compared to those from photoionization or non-equilibrium ionization. This would make some sense since CIE can be caused by shock fronts which would logically conclude with

different parts of the cloud being different temperatures (and thus having non-aligned HI and OVI components). Since the temperatures are too high to perfectly fit CIE in many cases, the Type 2 systems do not accurately fit any of the ionization possibilities. This result is consistent with Tripp et al. (2008) who found that aligned systems alone had $logT < 5.0$ for 62% of the systems. However, when both types of systems were considered, the cool fraction ($logT < 5.0$) dropped to 30%. This indicates that the non-aligned systems found in this study had higher temperatures than the aligned systems (though exactly how much higher is not reported in Tripp et al. (2008)).

With this analysis, it is important to recognize that all of these inferred temperatures were calculated under the assumption that the distribution of non-thermal b-values does not change between the Aligned and Non-Aligned systems. While evidence has been given that this is a fair assumption to make (see Section 4.3.1), it is still an assumption and has not been proven. Furthermore, these temperatures – both the ones calculated for the Type 1 systems and the ones inferred for the Type 2 systems – were found by assuming a single-component structure for the absorption features wherever possible. This means that most likely these features have the largest width possible which leads to higher temperatures estimates (since broad lines correspond to larger b-values which is proportional to temperature). Therefore, these temperature values are strictly upper limits, and may be lowered if multiple components were assumed for the original absorption features.

A final interesting result is that neither the Aligned temperatures (Figures 4.3 and 4.5) nor the Non-Aligned temperatures (Figures 4.7 – 4.9) show any correlation to the physical parameters of the clouds. Specifically, the lack of correlation between either Type 1 or 2 absorber temperatures and their column densities (Figures 4.3 and 4.8) means that both strong and weak absorbers (high and low *logN* respectively) can be hot. This is contrary to the assumed idea that strong absorbers are cool (which comes from the fact that ionization fraction is dependent on temperature).

5.2 Conclusion

This study probes the Warm-Hot Intergalactic Medium using COS/HST measurements of different absorber systems. We started with observations of absorbers containing both HI and OVI and separated them into two categories: systems where the HI and OVI were present at similar velocities (Type 1, Aligned) and systems where the two elements were at significantly different velocities and were therefore part of different gas clouds (Type 2, Non-Aligned). This is the largest sample of OVI absorbers that has been analyzed with this methodology, beginning with 259 OVI systems which were then separated into 203 Type 1s and 31 Type 2s.

These systems were separated because only the Type 1 systems had the possibility of HI and OVI being contained within the same cloud, and if they were in the same cloud then a temperature for that system could be computed. Temperatures were calculated for the Aligned systems and a distribution of temperatures significantly lower than expected was found. It is commonly thought that absorbers should be ionized partially due to photoionization and partially due to collisional ionization (despite the percentage of each being subject to much debate). However, the temperatures found here were too low to be due to collisional ionization in most cases, and are probably caused by photoionization or non-equilibrium ionization.

While the Type 1 systems are the only ones with the possibility of calculating accurate individual temperatures, certain assumptions can be made which allow an inferred temperature to be found for the Type 2 systems. Assuming that the only difference between the Aligned and Non-Aligned systems are their thermal values (which the evidence does point to), it can be assumed that the distribution for the non-thermal b-values is consistent from Type 1s to Type 2s. A median b_{NT} value found from the Type 1 data was applied to the Type 2 data in order to infer their temperatures. The OVI temperature distribution found here was much higher than that of the Type 1 systems, while the HI temperature distribution is lower –

typical of the photoionized Lyα forest ($T = 10^{3.5} – 10^{4.5}$). Therefore, the Non-Aligned systems are more likely to be collisionally ionized than the Aligned systems.

5.3 Possible Future Work

There are many possible courses of action from here in order to improve the work already done on the study of the WHIM. A better understanding of the systematic errors and biases of this sample would help improve knowledge of how this data is possibly the upper temperature limit. Specifically, the systematic errors on the linewidths (the b-values) needs to be closely examined. This could include, but is not limited to, considering the effects of choosing multiple components over single component fits for the absorption features. Another piece of work that should be done is comparing this study to simulation data as it could help test the accuracy of simulations and possibly improve their observational inputs.

In terms of the overall investigation of the WHIM, there are two major areas which need more research. The first is that there is a need for detections of lower column density systems ($logN \leq 13$) in order to have a more complete understanding of the WHIM gas. The second is that while the WHIM consists of gas in the temperatures range of $10^5 – 10^7$ K, OVI can only probe the lower portion of this range ($10^5 – 10^6$ K). Therefore, to fully understand the WHIM, the upper part of this range needs to be examined. This can be done using OVII as a probe, but it requires X-ray telescopes have poor velocity resolution. Therefore, once X-ray telescopes become better developed, using OVII to probe the WHIM would greatly improve the community's understanding of the baryon distribution of the IGM.

References

Cen, R., & Fang, T. (2006). Where Are the Baryons? III. Non-Equilibrium Effects and Observables. *The Astrophysical Journal, 650*(2), 573-591. doi:10.1086/506506

Danforth, C. W., Keeny, B. A., Tilton, E. M., Shull, J. M., Stocke, J. T., Stevans, M., . . . Osterman, S. N. (2016). An HST/COS Survey of the Low-redshift Intergalactic Medium. I. Survey, Methodology, and Overall Results. *The Astrophysical Journal, 817*(2), 111-139. doi:10.3847/0004-637X/817/2/111

Danforth, C. W., & Shull, J. M. (2005). The Low- z Intergalactic Medium. I. O vi Baryon Census. *The Astrophysical Journal, 624*(2), 555-560. doi:10.1086/429285

Danforth, C. W., & Shull, J. M. (2008). The Low-z Intergalactic Medium. III. H I and Metal Absorbers at z < 0.4. *The Astrophysical Journal, 679*(1), 194-219. doi:10.1086/587127

Fukugita, M., Hogan, C. J., & Peebles, P. J. (1998). The Cosmic Baryon Budget. *The Astrophysical Journal, 503*(2), 518-530. doi:10.1086/306025

Gnat, O., & Sternberg, A. (2007). Time-Dependent Ionization in Radiatively Cooling Gas. *The Astrophysical Journal Supplement Series, 168*(2), 213-230. doi:10.1086/509786

Green, J. C., Froning, C. S., Osterman, S., Ebberts, D., Heap, S. H., Leitherer, C., . . . Wilkinson, E. (2011). The Cosmic Origins Spectrograph. *The Astrophysical Journal*. doi:10.1088/0004-637X/744/1/60

Haardt, F., & Madau, P. (2012). Radiative Transfer in a Clumpy Universe. IV. New Synthesis Models of the Cosmic UV/X-Ray Background. *The Astrophysical Journal, 746*(2), 125-145. doi:10.1088/0004-637X/746/2/125

Haehnelt, M. G., Madau, P., Kudritzki, R., & Haardt, F. (2001). An Ionizing Ultraviolet Background Dominated by Massive Stars. *The Astrophysical Journal, 549*(2). doi:10.1086/319170

O'Meara, J. M., Burles, S., Prochaska, J. X., Prochter, G. E., Bernstein, R. A., & Burgess, K. M. (2006). The Deuterium-to-Hydrogen Abundance Ratio toward the QSO SDSS J155810.16-003120.0. *The Astrophysical Journal, 649*(2), L61-L65. doi:10.1086/508348

Savage, B. D., Kim, T., Wakker, B. P., Keeney, B., Shull, J. M., Stocke, J. T., & Green, J. C. (2014). The Properties of Low Redshift Intergalactic Ovi Absorbers Determined From High S/N Observations of 14 Qsos with the Cosmic Origins Spectrograph. *The Astrophysical Journal Supplement Series, 212*(1), 8. doi:10.1088/0067-0049/212/1/8

Shull, J. M., Smith, B. D., & Danforth, C. W. (2012). The Baryon Census in a Multiphase Intergalactic Medium: 30% of the Baryons May Still Be Missing. *The Astrophysical Journal, 759*(1), 23-38. doi:10.1088/0004-637X/759/1/23

Spergel, D. N., Bean, R., Doré, O., Nolta, M. R., Bennett, C. L., Dunkley, J., . . . Wright, E. L. (2007). Three-Year Wilkinson Microwave Anisotropy Probe (WMAP) Observations: Implications for Cosmology. *The Astrophysical Journal Supplement Series, 170*(2), 377-408. doi:10.1086/513700

Stocke, J. T., Keeney, B. A., Danforth, C. W., Syphers, D., Yamamoto, H., Shull, J. M., . . . Kacprzak, G. G. (2014). Absorption-Line Detections of 10^5-106 K Gas In Spiral-Rich Groups Of Galaxies. *The Astrophysical Journal, 791*(2), 128. doi:10.1088/0004-637x/791/2/128

Sutherland, R. S., & Dopita, M. A. (1993). Cooling Functions for Low-Density Astrophysical Plasmas. *Astrophysical Journal Supplement Series, 88*(1), 253-327. doi:10.1086/191823

Tepper-García, T., Richter, P., Schaye, J., Booth, C. M., Vecchia, C. D., Theuns, T., & Wiersma, R. P. (2011). Absorption Signatures of Warm-Hot Gas at Low Redshift: Ovi. *Monthly Notices of the Royal Astronomical Society, 413*(1), 190-212. doi:10.1111/j.1365-2966.2010.18123.x

Tripp, T. M., Sembach, K. R., Bowen, D. V., Savage, B. D., Jenkins, E. B., Lehner, N., & Richter, P. (2008). A High-Resolution Survey of Low-Redshift QSO Absorption Lines: Statistics and Physical Conditions of O vi Absorbers. *The Astrophysical Journal Supplement Series, 177*(1), 39-102. doi:10.1086/587486